Aquaculture 561 (2022) 738697

Contents lists available at ScienceDirect

Aquaculture

journal homepage: www.elsevier.com/locate/aquaculture

Rib abnormalities and their association with focal dark spots in Atlantic salmon fillets

Raúl Jiménez-Guerrero [a,*], Grete Baeverfjord [b], Øystein Evensen [c], Kristin Hamre [d], Thomas Larsson [e], Jens-Erik Dessen [e], Kjellrun-Hoås Gannestad [b], Turid Mørkøre [a,e]

[a] Department of Animal and Aquacultural Sciences, Norwegian University of Life Sciences, NO-1432 Ås, Norway
[b] Nofima, NO-6600 Sunndalsøra, Norway
[c] Department of Paraclinical Sciences, Faculty of Veterinary Medicine, Norwegian University of Life Sciences, NO-1433 Ås, Norway
[d] Department of Feed and Nutrition, Institute of Marine Research, NO-5005 Bergen, Norway
[e] Nofima, NO-1432 Ås, Norway

ARTICLE INFO

Keywords:
Fish farming
Rib fracture
Rib morphology
Melanin spots
Welfare

ABSTRACT

Focal dark spots (DS) represent the most common quality problem in farmed Atlantic salmon (*Salmo salar* L.). DS are predominantly located in the cranio-ventral region of the fillet, that is characterized by the presence of ribs. The current study explores the possible association between abnormal rib morphology and DS types and the frequency of rib abnormalities in the rib cage by X-ray imaging. The fish used were salmon from a common smolt group that were sampled in freshwater (smolt farm) and subsequently two, five, eight and 14 months after sea transfer to small-scale land-based tanks or commercial sea-cages. Large size wild salmon were used as additive. Rib abnormalities were found in most fish, with a consistent number of four abnormalities per rib cage side of smolts, land-based and wild salmon. After transfer from freshwater to sea-cages, there was an abrupt increase from four to 10 abnormal ribs per rib cage side, mainly explained by low-density and shorter ribs. The number of abnormal ribs stabilized in further samplings at around eight abnormalities per rib cage side. In contrast to wild salmon, abnormalities in farmed salmon were symmetrically concentrated in the center of the rib cage in mid and distal parts of ribs, where also most DS were concentrated. No typical black DS were observed in smolts, salmon farmed in land-based tanks or wild salmon. Two months after transfer to sea-cages, 15% of the salmon had fillet-red DS, while fillet-black DS were observed five months after sea transfer (30%). The prevalence of fillet-red DS oscillated between 15 and 3% during the seawater phase, while fillet-black DS increased until the eighth month after seawater transfer, stabilizing in further samplings at 43–45%. The prevalence of rib abnormalities was 1.6 times higher in fillet-black DS than in control tissue, and 2 times higher for peritoneum DS, principally because of various forms of bent-, and broken ribs. There was an association between rib abnormalities and DS, although additional factors influenced the final DS phenotype. Preventing damaging incidents in the late smolt phase and sea-cage operations can likely reduce the prevalence of abnormal ribs and DS.

1. Introduction

Focal dark spots (DS) represent the most common fillet quality problem in all regions globally with significant farming of Atlantic salmon (Nordberg, 2018), affecting 16% of marketable sized fish, and causing 9–67% price losses, depending on the intensity and size of the discoloration (Färber, 2017). Most fillet DS are about 3 cm wide with brown/black discoloration, but spots can also be reddish, or diffuse grayish covering larger areas (Mørkøre, 2012). DS are principally concentrated in the cranio-ventral region of the fillet, under the parietal peritoneum from ventral myocommata number 12 to 20 (Mørkøre, 2012; Mørkøre et al., 2015). Histological examination of DS has revealed degeneration and necrosis, fibrosis and granulomatous inflammation containing varying numbers of melano-macrophages (Larsen et al., 2012) of unclear etiology. Koppang et al. (2005), concluded that DS are an unpredictable side-effect of vaccination, while Bjørgen et al. (2015) proposed that *Piscine orthoreovirus* (PRV) is a premise for the development of DS. On the other hand, Krasnov et al. (2016) pointed to chronic

* Corresponding author at: Department of Animal and Aquacultural Sciences, Norwegian University of Life Sciences, NO-1430 Ås, Norway.
E-mail address: raul.jimenez.guerrero@nmbu.no (R. Jiménez-Guerrero).

https://doi.org/10.1016/j.aquaculture.2022.738697
Received 17 February 2022; Received in revised form 1 August 2022; Accepted 2 August 2022
Available online 6 August 2022

inflammation initiated by trauma without specific causative agents.

The anatomical region where the majority of DS are found is characterized by relatively high fat deposits (Aursand et al., 1994; Zhol et al., 1995), the presence of ribs (pleurapophysis) (De Clercq et al., 2017), and a thin muscle layer that may be susceptible to mechanical deformations. Long bone fractures and phases of the healing processes have been described in wild and farmed non-salmonid fish species (Fjelldal et al., 2020; Fjelldal et al., 2018; Horton and Summers, 2009; Tomecka et al., 2019). In farmed salmonids, rib abnormalities have been observed in form of sigmoid deviations associated with phosphorous deficiency (Baeverfjord et al., 1998). Gislason et al. (2010) reported supernumerary ribs due to dominant mutations. There is no literature investigating the association between ribs abnormalities and DS.

This study aimed to explore the association between rib abnormalities and DS of the abdominal wall of Atlantic salmon. This was done by characterizing normal and deviant rib bone morphology, and DS of salmon in freshwater and subsequently throughout the seawater grow-out phase in land-based tanks and commercial sea-cages until harvest (3.2–4.5 kg). Further, rib abnormalities and occurrence of DS were studied in large wild salmon as reference group.

2. Material and methods

2.1. Fish material

The fish material used were farmed and wild Atlantic salmon (*Salmo salar* L.). The farmed salmon (S0; Benchmark Genetics Norway, Bergen, Norway, line: trio QTL PD/IPN/Lice) were obtained from a commercial smolt producer making use of freshwater recirculation aquaculture technology (RAS) (Belsvik, Lerøy Midt, Hemne, Norway). The fish were farmed at the commercial RAS facility until smoltification and transferred to seawater in September 2018 (360,000 fish; 100 g), or they were transferred to flow-through land-based 0.7 m^3 tanks at the Research Station for Sustainable Aquaculture (Nofima, Sunndalsøra, Møre and Romsdal, Norway) as 20 g pre-smolts (June 5th 2018; 2000 fish). The salmon at the RAS facility were vaccinated July 2018 using Alpha ERM® salar bath treatment, and Alpha JECT® micro 6 by machine injection (PHARMAQ AS, Overhalla, Norway). The fish kept in land-based tanks were not vaccinated. Smoltification was induced with artificial photoperiod regimes (6 weeks winter signal of 12:12 Light:Dark hours, post and prior to 24 L:0D) at both pre-smolt farming locations. The smoltification status was checked by conducting a seawater challenge test, followed by determination of plasma osmolality, chloride content, and gill Na^+,K^+-ATPase activity (Clarke et al., 1996) before sea transfer in September 2018 when the average weight was 100 g. The smolts at the land-based facility were transferred to 3.2 m^3 tanks, supplied with UV-treated seawater from Tingvollfjorden (pumped from 40 m depth). The smolts from the commercial RAS facility were transported by a well-boat and distributed into four open commercial-sized sea-cages (120 m circumference, 40 m depth) with 80,000 fish in each cage at Nofima commercial-scale research and development (R&D) facility in Tingvollfjorden (Lerøy Midt AS, Gjemnes, Norway; 62°North, 8° 5′ 0″ East east). The distance between the farming locations was 45 km, i.e., the land-based tanks and sea-cages were supplied with seawater from the same fjord. The fish in sea-cages were mechanically deloused using the SkaMik 1.5 system (SkaMik AS, Ottersøy, Norway) in September and October 2019.

Both fish groups were fed the same standard grower feed, with pellet size and feed composition adjusted to fish size according to the recommendation from the feed producer (BioMar, Trondheim, Norway).

As additive material, wild Atlantic salmon by-caught in the sea outside Finnmark, Norway April 2018 and in the Namsen River, Trøndelag, Norway by net in June 2019 were purchased from a fishmonger and shipped frozen and on ice, respectively to Nofima AS, Ås, Norway for analyses.

2.2. Sampling of fish material

Farmed salmon were sampled for analyses prior to seawater transfer after vaccination at the commercial smolt farm and four times throughout the seawater rearing phase in land-based tanks and sea-cages (Table 1). At each sampling point, fish representing the average weight of the rearing units were anesthetized using MS-222 (Metacaine 0.1 g l − 1; Pharmaq Ltd., Hampshire, UK) or Benzoac (Benzoac® 2 ml × 150 10 L-1, ACD Pharmaceuticals AS, Leknes, Norway) and killed by a lethal blow to the head before bleeding out, evisceration and filleting by hand. Left and right rib cages of each salmon (farmed and wild) were examined by X-ray.

In November 2019, the ventricle tip of 32 salmon farmed in land-based tanks and sea-cages were sampled in RNA later® for real-time RT-PCR analysis of *Piscine orthoreovirus-I* (PRV—I) (PatoGen AS, Ålesund, Norway).

2.3. Radiography

Rib morphology changes with growth were studied by X-ray of farmed salmon rib cages at each sampling timepoint (Table 1). Wild salmon caught in freshwater were additive, and not part of the time-based study. Left and right sides of rib cages were placed on trays before X-ray analyses using an IMS Giotto mammography equipment (Giotto, Pontecchio Marconi, BO, Italy) (Fig. 1A). The image resolution was 20 pixels per mm^2, with exposure at 22 kV and 100 mAs. X-ray images were recorded on coated photo-reactive phosphorous Fujifilm Computed Radiography (FCR) Imaging Plates (Fujifilm, Tokyo, Japan). Plates were read using FCR Profect Reader (Fujifilm, Tokyo, Japan).

General rib morphology and abnormalities were evaluated from the first fully developed rib (vertebra number 4) to 22nd rib at three different positions of each rib; proximal, mid, and distal (Fig. 1A). Before rib evaluation, a classification system was developed based on the type

Table 1
Fish material description and purpose.

Environment	Sampling time	Body weight (kg)	n		
			DS prevalence	Rib cage X-ray	NQC bone analysis
Wild-Seawater	April 2019	2.2 ± 0.2	21		
Wild-Freshwater	June 2019	5.1 ± 0.2	15	15	15
Smolt farm - Freshwater	August 2018	0.1 ± 0	20	20	
Land-based tank - Seawater	November 2018	0.3 ± 0	15	15	
Land-based tank - Seawater	February 2019	0.8 ± 0	15	15	
Land-based tank - Seawater	May 2019	1.4 ± 0	15	15	
Land-based tank - Seawater	November 2019	3.2 ± 0	60	23	15
Sea-cage - Seawater	November 2018	0.5 ± 0	60	10	
Sea-cage - Seawater	February 2019	1.2 ± 0	60	30	
Sea-cage - Seawater	May 2019	2 ± 0	60	10	
Sea-cage - Seawater	November 2019	4.5 ± 0	113	23	10

DS, focal dark spots.
NQC, Norwegian quality cut.
Weight values are shown as mean ± SEM.

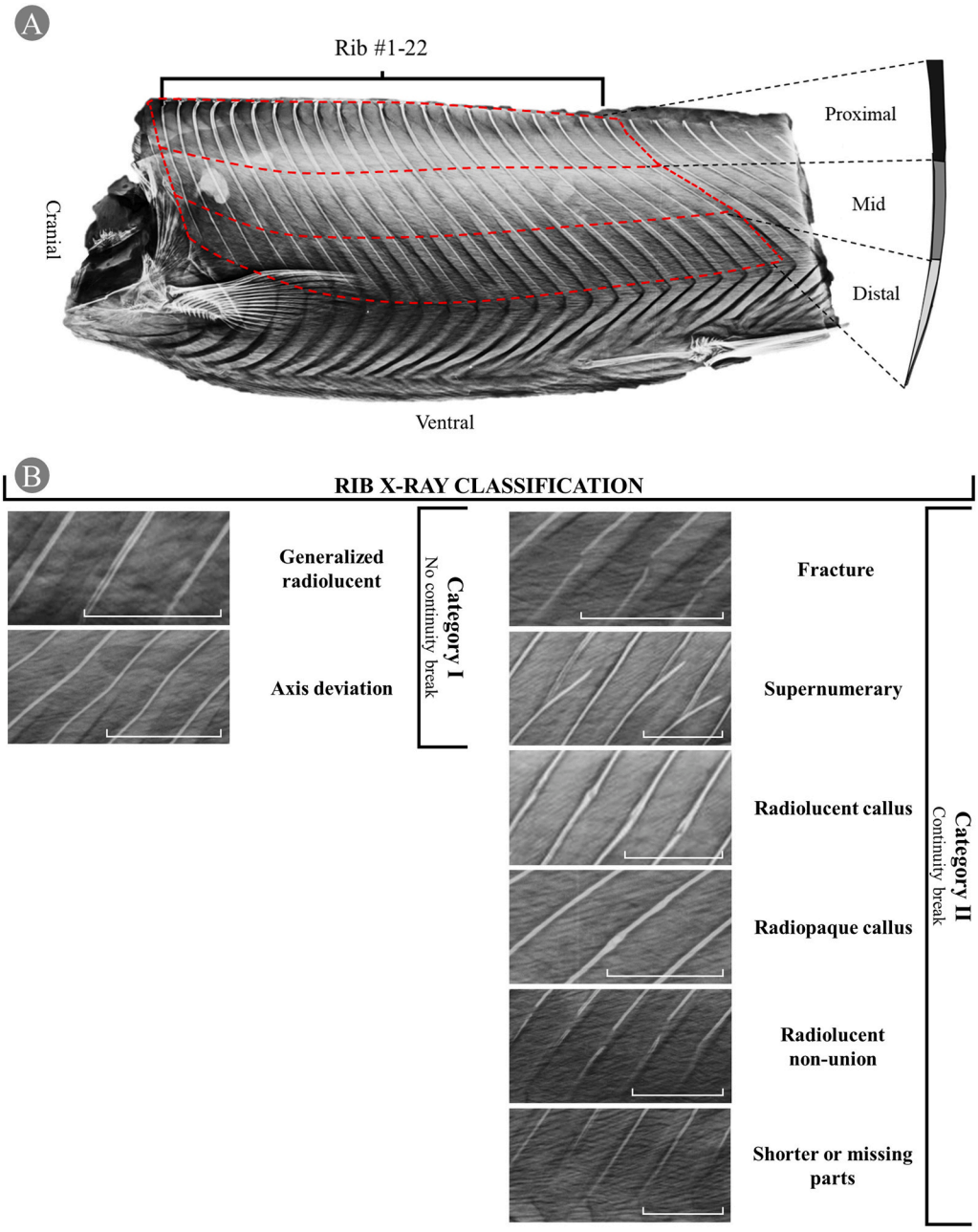

Fig. 1. Method for salmon rib morphology evaluation in rib cage of Atlantic salmon. A) Fillet map evaluation. B) Classification system for rib abnormalities. White restricted bars on the bottom right corner of each picture show the scale, set to 1 cm.

of abnormalities observed in rib cages from different sampling points and environments (salmon, $n = 176$) and existing literature (Fjelldal et al., 2020; Gislason et al., 2010; Khurana, 2009; Tomecka et al., 2019), aiming to identify different abnormality types and severity (Fig. 1B). Assuming a post-traumatic mechanical disturbance of local tissue in continuity breaks, abnormalities were classified into two distinct categories: rib abnormalities with no continuity break (Category I) and ribs with or related to continuity breaks (Category II). Category I was further divided into two sub-categories: 1) generalized radiolucent at mid-distal parts with an increase of rib diameter and 2) axis deviations. Category II was divided into six sub-categories: 1) fracture, 2) supernumerary ribs, where free terminal rib fragments could continue their longitudinal growth independently, 3) radiolucent callus, 4) radiopaque callus as normal healing responses in long bones, 5) radiolucent non-unions, as atrophic non-unions with resorption of free fragments, and 6) shorter or missing rib parts. Rib axis deviations were not included in total sums of the time-based study of rib cages to minimize artifacts given their vulnerability during handling and filleting different fish sizes. However, rib axis deviations were considered in the targeted study of DS and control areas, since the risk of artifacts is considered minimal for the dissected small DS areas.

Morphology of ribs attached to dark-stained skeletal muscle and peritoneum was characterized using the same classification system (Fig. 1) and compared to their non-pigmented surroundings.

2.4. Targeted study of DS

DS observed in left and right fillets of sea-cage farmed fish (Fig. 2) were macroscopically examined and categorized from seawater transfer to harvest (Lerøy processing plant, Hitra island, Norway) (fillet-red DS, $n = 23$; fillet-black DS, $n = 94$; peritoneum DS, $n = 63$). Due to the low number of detected fillet-red DS at the smolt farm and land-based tanks,

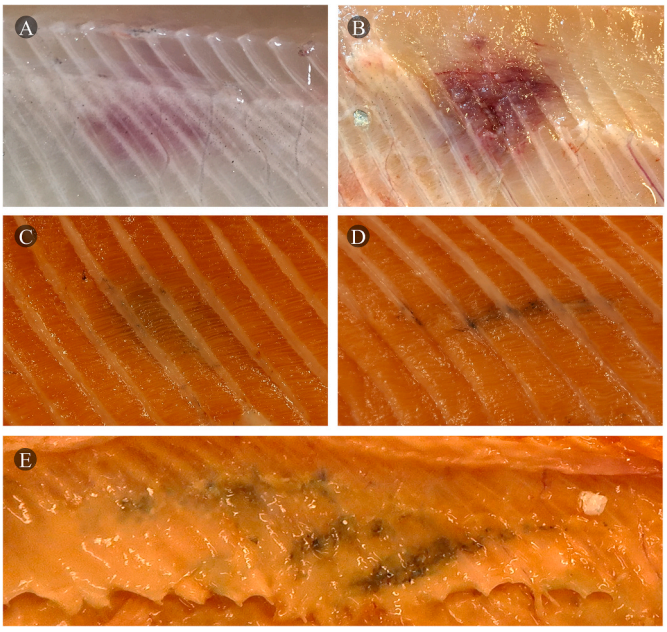

Fig. 2. Illustration of different focal dark spots (DS) of Atlantic salmon fillets. A) Fillet-red DS of salmon in freshwater (smolts), B) fillet-red DS after seawater transfer, C) fillet-black DS of salmon in seawater with low- and D) high aspect ratio, and E) peritoneum DS. (For interpretation of the references to color in this figure legend, the reader is referred to the web version of this article.)

they were not included in statistical analysis (Fig. 2), though they were evaluated and examined by X-ray. If the fish presented several DS (e.g., left and right fillet, or fillet and peritoneum), they were studied as independent focal discolorations. Randomly selected DS from sea-cage fish were chosen for X-ray examinations, (fillet-red DS, $n = 15$; fillet-black DS, $n = 76$; peritoneum DS, n = 63). From harvest size fish, randomly selected black DS with adjacent ribs and peritoneum ($n = 46$) were put in formalin (10% phosphate-buffered formalin, pH 7.0, >3 days at 4 °C). Rib and peritoneum samples without macroscopic evidence for DS were sampled as controls ($n = 20$) from the same fish between rib number 11 to 14 at the mid position of the rib and placed in formalin. Based on macroscopic appearance and X-ray examinations, formalin-fixed samples were selected for micro-CT (control, n = 9; black DS, $n = 21$), followed by histopathology. Additional ribs ($n = 5$) from adult wild fish were sampled and placed in formalin for complementing morphological descriptions.

2.5. Evaluation of fillet DS

A novel method for evaluating red and brown/black DS of the cranio-ventral fillet region was developed to facilitate objective continuous measurements of discoloration and area separately, while correcting for different fish sizes (Fig. 3). After filleting, the peritoneum and rib cage were carefully trimmed to visualize aberrant DS. Pictures of the cranio-ventral fillet region with visible DS were taken using a Canon PowerShot G7 X Mark II (Canon Inc., Tokyo, Japan), 5472 × 3648 resolution, using "Auto" mode with flash off, and ambient lighting. Images of skeletal muscle DS were further processed, and fillet-red DS were excluded at slaughter-exclusive explorations due to insufficient available X-rayed material ($n = 3$).

DS features based on the photographic images included: rib numbers corresponding to discolored myomeres, absolute distance from the horizontal septum (mid-line) to DS center (cm), absolute area (mm^2), maximum horizontal (X) and vertical length (Y) to estimate aspect ratio (AR = X/Y) as a scale-independent factor; number of affected myomeres, and color as darkness intensity (Fig. 3). Inputs for estimating aspect ratio were assessed using the ImageJ software (v1.52s, U. S. National Institutes of Health, Bethesda, USA), and DS area was calculated assuming that most DS have an ellipse-like shape (DS area = π * a * b). The number of affected myomeres (starting from 0.2 when it affects only one myocommata) was transformed (times 5) to relative DS length to avoid values between 0 and 1, which might disturb area calculations. Thus, *a* equals 0.5 * Relative DS length, while *b* equals 0.5 * Relative DS length/AR. The relative DS area was transformed to DS area as myomere^2 units. Darkness intensity was determined at the DS core using a scale with five levels, from 0 (no visible dark pigmentation) to 4 (intense and homogeneous dark pigmentation with or without visible scar formation). DS level was calculated by multiplying the DS area by their DS darkness intensity (Fig. 3).

2.6. Micro computed tomography (micro-CT)

Samples were scanned at the Nofima center of nutrition and feed technology (Kjerreidviken, Bergen, Norway) using a Skyscan 1275 X-ray microtomograph (Bruker micro-CT, Kontich, Belgium) by a source voltage of 50 kV and 200 μA current, with exposure time set to 46 ms. 360-degree images, pixel size 20–28 μm, and rotation step of 0.3°. Image reconstruction was done using NRecon (v. 1.7.3.1, Bruker micro-CT, Kontich, Belgium), with the following parameters: 0 smoothing, 5 ring artifact reduction, 25 beam hardening correction, post alignment adjusted for every sample, and CS to 0.000000–0.030000. After scanning, 3D models for rib bones were made with CTAn (v.1.17.7.2, Bruker, Kontich, Belgium). Video files for each sample were created using CTVox (v.3.3.0, Bruker, Kontich, Belgium). The bone tissue threshold was set manually for every sample.

2.7. Vertebra mineral analysis

Selected macrominerals in vertebrae of wild and slaughter size land-based and sea-cage farmed salmon were analyzed in the axial skeleton between the caudal end of the dorsal fin and the gut, commonly termed the Norwegian quality cut (NQC). The vertebrae were cleaned for surrounding soft tissue and trimmed for haemal and neural spines. Thereafter samples were pooled and homogenized in groups of five fish (per rearing unit farmed salmon). Analyses of the macrominerals (Ca, K, Mg, P) was performed using acid digestion, extraction, and inductive coupled plasma-mass spectrometry (ICP-MS) according to Liaset et al. (2003).

2.8. Statistics

Statistical analyses were conducted using R software (v. 4.0.3, R Core Team, Vienna, Austria). Figures were produced using Microsoft® Excel® software (v. 16.0.12527.21294, Microsoft Corporation, Redmond, United States). Parametric responses were modeled using the "lm()" R function, while "glm()" adjusted for Poisson or binomial distribution when dealing with non-parametric responses. The pair-wise comparison was made using the "HSD.test()" R function with square root normalization of the response if possible when dealing with non-parametric distributions, or Wilcoxon signed rank test using the "pairwise.wilcox.test()" R function when diagnostic plots revealed no optimum distribution of residuals after transformation. Models were adjusted for unbalanced design when required. Results from vertebral mineral analyses were evaluated with SAS® (V9.4, SAS Institute Inc., Cary, US). No random effects were considered in the models. The significance level was set at $p \leq 0.05$, and results are presented as mean ± standard error (SEM).

2.9. Histopathology

Tissue samples in formalin were examined for pathological changes by light microscopy. Decalcification was performed by incubating the samples in 14% ethylenediaminetetraacetic acid (EDTA) for up to 48 h.

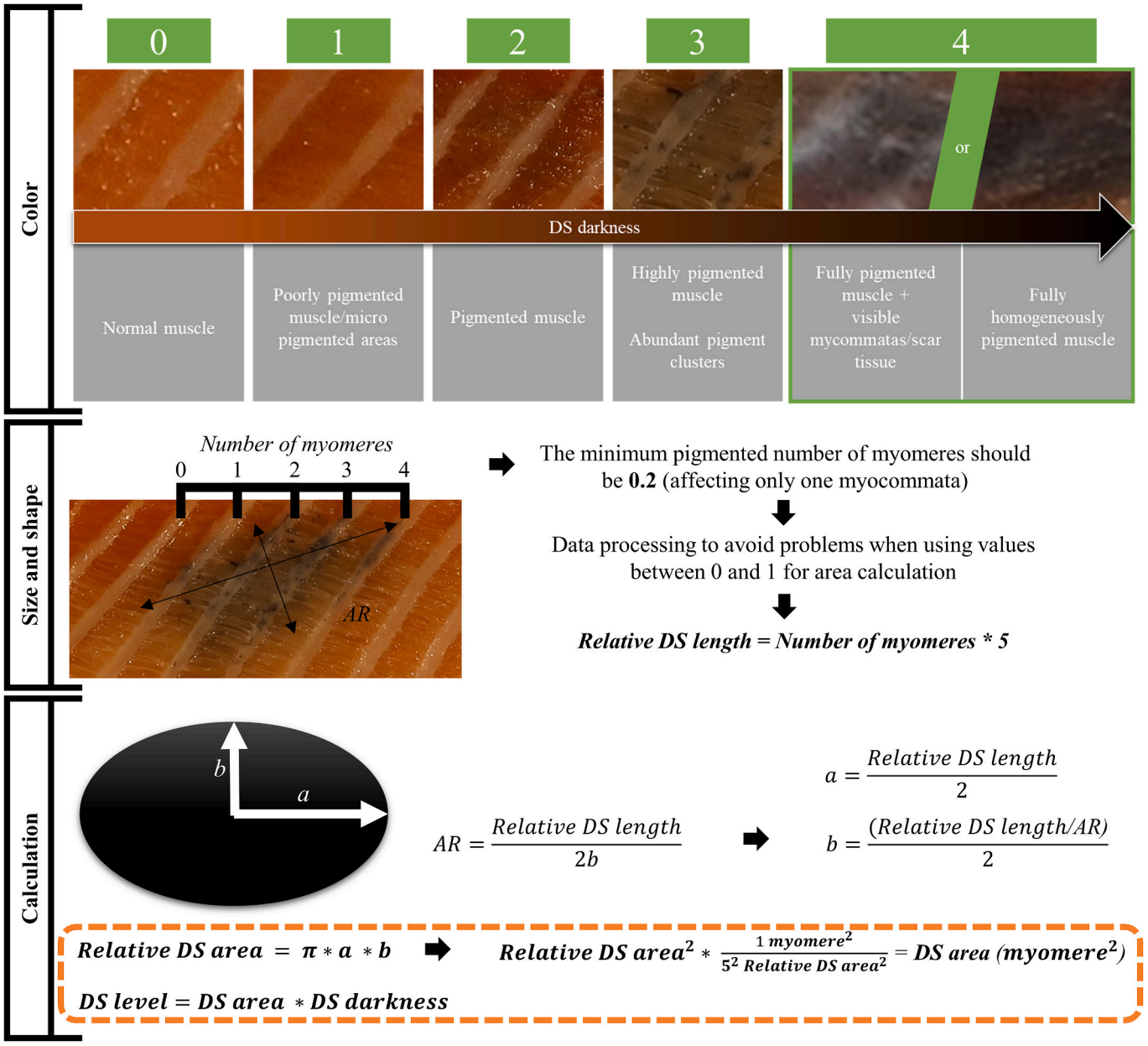

Fig. 3. Color scale and formula for quantification of targeted fillet DS area and DS level of Atlantic salmon fillets. Aspect ratio (AR) is calculated as the major horizontal axis's length divided by the DS minor vertical axis. The initial transformation for the number of myomeres to relative spot length, is corrected at the end of DS area calculation.

Samples were then embedded in paraffin wax and sectioned at 1.5–2 μm. Sections were mounted on glass slides and stained with haematoxylin and eosin. Slides were scanned at a resolution of 221 nm/pixel, with an image size of 126.720 × 87.296 pixels in a Nanozoomer digital pathology image (ndpi) format, and created in a NDP.scan 3.2.15. Images were examined and sampled using NDP.view.2 (v.2.7.43, Hamamatsu Photonics K·K, Hamamatsu, Japan).

3. Results

3.1. Rib morphology of rib cages

X-ray evaluations showed ventro-caudally orientation of the ribs in a decreasing angle towards the tail. Ribs changed the length gradually along the rib cage. The shortest rib, usually the first one and frequently missing, was found at the 3rd vertebra. Generally, the length of the ribs increased from vertebra number 3 to 9–12 counted from the head. The total number of ribs attached to the vertebra basiventral (non-vestigial ribs) was between 21 and 23.

X-ray evaluations showed all rib abnormality types in each studied environment, except for radiolucent non-unions, which were not found in wild fish (Table 2), and at least one rib abnormality was observed in every rib cage at any life stage and environment. The overall average rib abnormalities per rib cage side was four for wild salmon, salmon sampled at the smolt farm and land-based tanks. The salmon farmed in sea-cages had eight rib abnormalities per rib cage side on average, that was significantly higher from the other groups ($p \leq 0.01$). The abrupt increase in the number of rib abnormalities from the smolt farm (Aug. 2018) to two months after seawater transfer to sea-cages (Nov. 2018) ($p = 0.03$), was mainly due to an increased number of generalized radiolucent ribs (0.1 vs. 5.2; $p < 0.0001$) and shorter or missing rib parts (1.5 vs. 3.4; $p = 0.004$). The prevalence of generalized radiolucent ribs was

Table 2
Number of different rib abnormalities per rib cage side for wild and farmed Atlantic salmon before and after seawater transfer to land-based tanks and sea-cages.

Abnormality group n	Wild	Smolt farm	Land-based tank				Sea-cage			
	Jun. 2020	Aug. 2018	Nov. 2018	Feb. 2019	May. 2019	Nov. 2019	Nov. 2018	Feb. 2019	May. 2019	Nov. 2019
	15	20	15	15	15	23	10	30	10	23
Category I - No continuity break										
Generalized radiolucent	1.3 ± 0.5^{bcd}	0.1 ± 0.1^{d}	1.7 ± 0.5^{bc}	0.7 ± 0.2^{bcd}	1.1 ± 0.5^{bc}	0.3 ± 0.1^{cd}	5.2 ± 1.4^{a}	1.7 ± 0.4^{bc}	2.2 ± 0.7^{b}	1.3 ± 0.3^{bcd}
Axis deviation	5.7 ± 1.1^{cde}	6.7 ± 0.8^{bc}	6.5 ± 1.2^{bcd}	4.8 ± 0.8^{de}	4.2 ± 0.9^{e}	12.9 ± 1^{a}	7.1 ± 1.4^{bc}	1.2 ± 0.4^{f}	1.8 ± 0.6^{f}	8.2 ± 0.9^{b}
Any Category I	7 ± 1.2^{bcd}	6.8 ± 0.8^{bcd}	8.2 ± 1.3^{abcd}	5.5 ± 0.8^{cde}	5.3 ± 0.9^{cde}	13.1 ± 1.1^{a}	12.3 ± 2.1^{ab}	2.9 ± 0.6^{e}	4 ± 1de	9.5 ± 0.9^{abc}
Category II - Continuity break										
Fracture	0.3 ± 0.3	0.3 ± 0.1	0 ± 0	0 ± 0	0.1 ± 0.1	0.3 ± 0.2	0.3 ± 0.2	0.5 ± 0.2	0 ± 0	0 ± 0
Supernumerary	0.1 ± 0.1	0.1 ± 0.1	0.1 ± 0.1	0.1 ± 0.1	0.1 ± 0.1	0.2 ± 0.1	0.1 ± 0.1	0.6 ± 0.3	0.3 ± 0.3	0.2 ± 0.1
Radiolucent callus	1.1 ± 0.4^{ab}	0.1 ± 0.1^{b}	0.1 ± 0.1^{b}	0.1 ± 0.1^{b}	0.1 ± 0.1^{b}	1.4 ± 0.3^{a}	0.2 ± 0.2^{b}	0.1 ± 0.1^{b}	0.7 ± 0.4^{ab}	0.7 ± 0.2^{ab}
Radiopaque callus	0.5 ± 0.3^{b}	1.7 ± 0.3^{ab}	0.9 ± 0.4^{b}	0.5 ± 0.2^{b}	0.4 ± 0.2^{b}	0.7 ± 0.2^{b}	0.9 ± 0.4^{b}	1.2 ± 0.4^{b}	1.7 ± 0.5^{ab}	3 ± 0.5^{a}
Radiolucent non-union	0 ± 0	0.1 ± 0.1	0 ± 0	0.1 ± 0.1	0 ± 0	0 ± 0	0 ± 0	0.1 ± 0	0 ± 0	0 ± 0
Shorter or missing part	0.7 ± 0.3^{c}	1.5 ± 0.3^{bc}	1.4 ± 0.3^{bc}	1.2 ± 0.3^{bc}	1.3 ± 0.3^{bc}	1.5 ± 0.3^{bc}	3.4 ± 0.8^{a}	3.2 ± 0.4^{a}	2.7 ± 0.9^{ab}	2.6 ± 0.6^{ab}
Any Category II	2.7 ± 0.6^{b}	3.7 ± 0.5^{ab}	2.6 ± 0.7^{b}	2 ± 0.4^{b}	1.9 ± 0.4^{b}	4.1 ± 0.6^{ab}	4.9 ± 1.3^{ab}	5.7 ± 0.9^{ab}	5.4 ± 1.8^{ab}	6.5 ± 0.8^{a}

Values shown as mean ± SEM in the same row between environments and life stages with different letters are significantly different ($p \leq 0.05$).

the only abnormality type increasing two months after seawater transfer to land-based tanks (0.1 vs. 1.7; $p = 0.02$) (Table 2).

Time-based changes in seawater for the total number of rib abnormalities in fish from land-based tanks and sea-cages remained stable (Fig. 4). The main contributors for higher numbers in sea-cages were generalized radiolucent ribs and shorter or missing rib parts, although a decreasing tendency was observed from two months after seawater transfer to slaughter (5.2–1.4; $p < 0.0001$ and 3.4–2.6; $p = 0.8$, respectively). On the other hand, the prevalence of radiopaque callus increased during sweater phase (0.9–3; $p = 0.0005$) (Table 2). At harvesting, the number of shorter or missing rib parts and radiopaque callus were four and six times higher in farmed salmon in sea-cages than in wild salmon ($p = 0.002$ and $p < 0.0001$, respectively) (Table 2).

The total number of abnormalities per rib of salmon sampled at the smolt farm increased in the posterior direction to a maximum level of 0.4 at rib number 21 (Fig. 5A). The pattern changed two months after transfer to seawater to a consistent increasing tendency towards rib number 12–14, with a peak at each third rib. Thereafter, the prevalence of rib abnormalities decreased posteriorly for the salmon farmed in land-based tanks, while the prevalence of rib abnormalities continued to be high towards rib 19 for sea-cage farmed salmon (Fig. 5A) (Supplementary 1). The number of abnormalities per rib of sea-cage farmed salmon was consistently higher compared with salmon farmed in land-based tanks, reaching a maximum level of 1 and 0.75 rib abnormalities per rib of the cage side, respectively. At slaughter (Nov. 2019) (Fig. 5B), the rib abnormality pattern was similar in salmon farmed in sea-cages and land-based tanks, with an increasing frequency up to rib number 12 for both farming environments while decreasing gradually in the posterior direction. The wild salmon showed a non-consistent longitudinal pattern. Abnormalities increased in the proximal-distal direction of the ribs for all fish groups, with significantly highest values for salmon farmed in sea-cages compared with wild ($p = 0.04$), and salmon farmed in land-based tanks ($p = 0.04$) (Fig. 6).

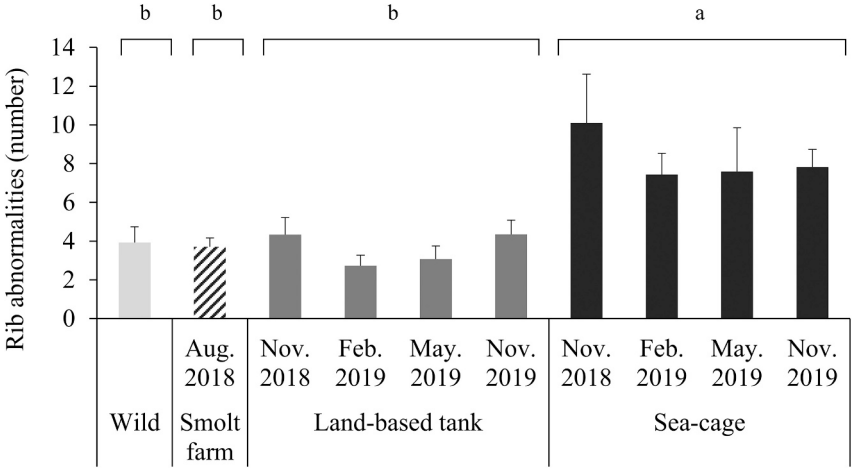

Fig. 4. Life stage and growing environment effects in the number of rib abnormalities per rib cage side for wild, and farmed Atlantic salmon before and after seawater transfer to land-based tanks and sea-cages. Significant differences between groups are indicated by different letters over the top brackets ($p \leq 0.05$). Data are presented as non-transformed mean ± SEM, $n = 15, 20, 68, 73$, for wild, smolt farm, land-based tank, and sea-cage groups, respectively.

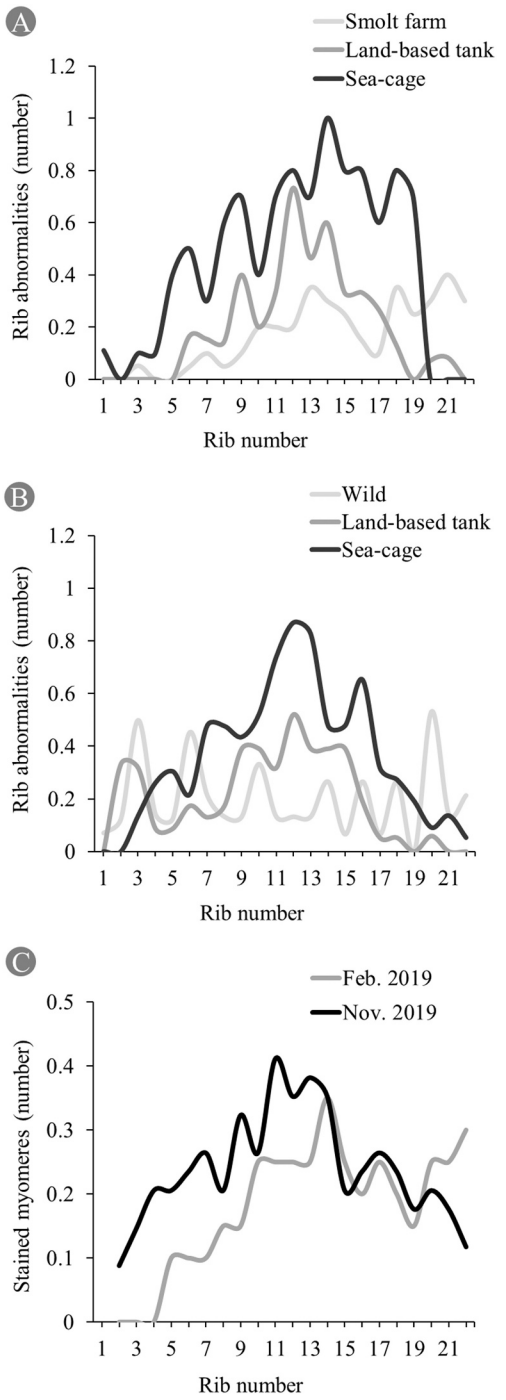

Fig. 5. Distribution of rib abnormalities and fillet DS along the rib cage of Atlantic salmon. A) farmed salmon in freshwater (smolts after vaccination, 80 g; $n = 20$) and two months after (Nov. 2018) seawater transfer to sea-cages (0.5 kg; $n = 10$) or land-based tanks (0.3 kg; n = 15). B) Slaughter size wild (5.1 kg; n = 15) and farmed salmon in land-based tank (3.2 kg; $n = 23$) and sea-cages (4.5 kg; n = 23). C) Mean values for the number of stained myomeres per fillet of salmon five months after transfer to sea-cages (Feb. 2019, 1.2 kg; n = 20), and slaughter (Nov. 2019, 4.5 kg; $n = 34$).

3.2. Targeted study of DS

3.2.1. DS prevalence, distribution, and morphology

Fillet-black DS were only observed in salmon farmed in sea-cages and only five months following sea transfer (30% of fish) and onwards (43–45% of fish). At the first sampling following seawater transfer (body weight 0.5 kg), all fillet DS were red, but subsequently both fillet-red DS and fillet-black DS were observed (body weight 1.2–4.5 kg). Fillet-red DS in sea-cage fish followed a non-increasing prevalence ranging from 3 to 15% (Fig. 7). Fillet-red DS, determined as focal intramuscular hemorrhages, were detected at the smolt farm and land-based tanks only following seawater transfer. Focal peritonitis in the form of hyperemic areas was observed in some fish at the smolt farm near the vaccination site.

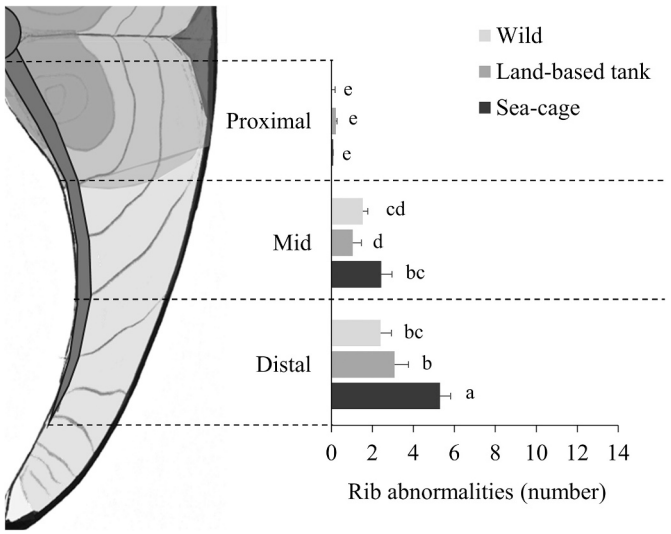

Fig. 6. Growing environment effects in the number of rib abnormalities at proximal, mid, and distal rib parts per rib cage side of slaughter size wild, and farmed Atlantic salmon using two rearing conditions after seawater transfer: land-based tank and sea-cage. Significant differences between groups and rib parts are indicated by different letters over the bars ($p \leq 0.05$). Data are presented as mean ± SEM, n = 15, 23, and 23 for wild, land-based tank and sea-cage farmed salmon, respectively.

At slaughter, 73% of salmon showed some form of DS (peritoneum and/or fillet). Peritoneum DS prevalence was 52%, and 79% of fillet DS were visible through the overlying peritoneum ($n = 33$). Diffuse dark pigmentation was observed in some parietal peritoneum areas in contact with voluminous organs (e.g., liver). Dark pigmentation was also observed in the adjacent peritoneum of rib terminal regions, where there

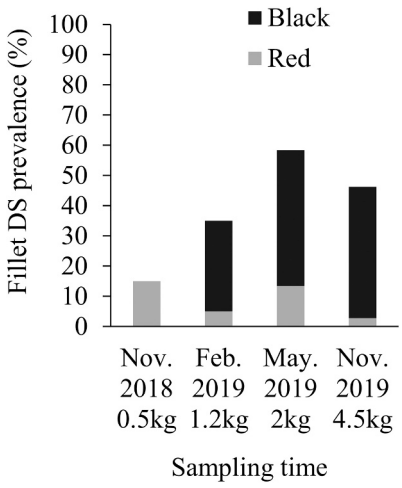

Fig. 7. Prevalence of focal black and red dark spots (DS) of fillets of Atlantic salmon farmed in sea-cages. The fish were sampled for analyses in Nov. 2018 ($n = 60$), Feb. 2019 (n = 60), May. 2019 (n = 60), and Nov. 2019 ($n = 113$). (For interpretation of the references to color in this figure legend, the reader is referred to the web version of this article.)

is a certain degree of rib motility.

The location of the DS in salmon fillets five months after seawater transfer to sea-cages (Feb. 2019) showed an increasing tendency towards rib number 14 where a maximum level of 0.34 stained myomeres was observed. Thereafter, the pattern oscillated between 0.15 and 0.3 myomeres in the posterior direction. At slaughter, the occurrence of fillet DS increased towards rib number 11–14 with 0.4 stained myomeres as maximum. The prevalence of fillet DS decreased gradually from rib 14–22 (Fig. 5C). Moreover, most of fillet DS were located at 3 cm bellow the horizontal septum, (mid rib parts), following a normal distribution from 0.9 cm (proximal rib parts) to 4.8 cm (distal rib parts).

Macroscopic evaluations revealed that fillet-red DS were consistently darker ($p = 0.0005$), relatively larger ($p = 0.04$), of higher level ($p < 0.0001$), and rounder ($p = 0.008$) than fillet-black DS (Table 3). Fillet-black DS area became larger in absolute terms (338 vs. 210 mm^2; $p = 0.03$), smaller relative to the fish size (2.4 vs. 6.5 $myomere^2$; $p < 0.0001$), flatter (4 vs. 1.7 aspect ratio; $p < 0.0001$), and lower intensity level (4.5 vs. 17.1 DS level; $p < 0.0001$) at harvesting than those first observed five months after seawater transfer. At harvesting, the appearance of fillet DS depended on where on the fillet the spot was located. The closer the DS was to the horizontal septum, the larger the relative DS area ($myomere^2$; $p = 0.02$), intensity level (DS level; $p < 0.0001$), and the rounder the shape (lower aspect ratio; $p < 0.0001$).

3.2.2. Relationship between DS and rib abnormalities

Besides a few ribs with axis deviations, no major X-ray findings compatible with rib fractures or other abnormalities associated with continuity break were observed in fillet-red DS of fish from the smolt farm and land-based tanks.

X-ray analysis of DS from all sampling times in sea-cages showed that the prevalence of rib abnormalities was significantly higher in peritoneum DS (79%) compared with the control tissue (40%) ($p = 0.002$), and the prevalence of rib abnormalities also tended to be higher in fillet-black DS (63%) ($p = 0.07$). The prevalence of rib abnormalities was lower of fillet-red DS (33%) compared with fillet-black DS ($p = 0.04$), but similar with control tissue (Table 3). Rib abnormality prevalence of fillet-black DS was higher at slaughter (72%; $n = 46$) than those first detected in five months after seawater transfer (41%; $n = 17$) ($p = 0.03$), and rib abnormalities in peritoneum DS followed the same trend (87 and 68%; $p = 0.08$). No differences were observed in relative prevalence for individual rib abnormality types among DS, except from higher prevalence of shorter or missing rib parts in fillet-black DS (43% vs. 6% of DS with rib abnormalities; $p = 0.02$) and peritoneum DS (59% vs. 6% of DS with rib abnormalities; $p = 0.0004$) five months after seawater transfer than at slaughter.

At slaughter, the difference between rib abnormality prevalence of peritoneum DS and fillet-black DS was not significant, but both were higher than control samples (40%) ($p = 0.0005$ and $p = 0.02$, respectively). Axis deviation was the most prevalent abnormality type in DS (76% of DS with rib abnormalities), followed by radiolucent callus and generalized radiolucent ribs (30–39% of DS with rib abnormalities). The relative prevalence for individual rib abnormality types between DS and control tissues did not differ significantly. Rib fractures, supernumerary ribs, radiolucent callus, and shorter or missing rib parts were not found in control tissues. These are called "DS-specific Category II" rib abnormalities, being present in 42% of DS samples with rib abnormalities at slaughter (Supplementary 2). Hence, the number of these most characteristic rib abnormalities in DS of the targeted study (either quantitively, axis deviations; or qualitatively, DS-specific Category II), were found to be similar in general rib cage evaluations of fish with none or any form of DS.

At slaughter, rib X-ray morphology in targeted fillet-black DS was compared against their DS features. Fillet-black DS with larger intensity levels had fewer presence of rib abnormalities ($p = 0.002$), and larger presence of the generalized radiolucent type ($p = 0.0007$) than lower intensity levels. In contrast to rounder DS, flattened phenotypes showed smaller relative DS area ($p = 0.02$) and larger presence rib abnormalities ($p = 0.0003$), especially axis deviations ($p < 0.0001$). Generally, flattened phenotypes presented a series of rib abnormalities in a linear pattern perpendicular to the rib direction.

Table 3
Discoloration and morphological characteristics of focal dark spots (DS) of fillets and peritoneum of Atlantic salmon sampled during the seawater period, and their associated rib abnormality prevalence. Fillet DS parameters are presented as pigment intensity (darkness score), shape (aspect ratio), relative area ($myomere^2$) and relative area times pigment intensity (DS level).

	Control*	Fillet-red DS	Fillet-black DS	Peritoneum DS
Darkness score	.	3.2 ± 0.2^{a}	1.8 ± 0.1^{b}	.
Aspect ratio	.	1.9 ± 0.4^{b}	3.1 ± 0.4^{a}	.
DS area ($myomere^2$)	.	5.5 ± 1.0^{a}	4.3 ± 0.5^{b}	.
DS level	.	19.2 ± 4.0^{a}	8.8 ± 1.2^{b}	.
Any rib abnormality (%)	40^{bc}	33^{c}	63^{b}	79^{a}

Values shown as prevalence or mean ± SEM in the same row with different letters are significantly different ($p \leq 0.05$).
* Control samples exclusively from slaughter.

3.3. PRV status

Heart samples of slaughter size farmed salmon showed positive results for PRV in all sampled individuals from sea-cages, while fish sampled in land-based tanks were negative for PRV.

3.4. Micro-CT and 3D model

The morphology of salmon ribs presents a tubular structure with bone processes ventrally oriented in the exterior surface of some proximal parts (Fig. 8A). Proximal cross-sectional ribs parts were flattened and laterally oriented, reaching deeper layers into the muscle wall, becoming increasingly rod-like and less integrated into the muscle wall at distal parts (Fig. 8A and B).

The 3D model for bone density of rib abnormalities from the DS-specific Category II group at distal (radiolucent non-union), mid (radiolucent callus), and mid-proximal (fracture) rib parts, presented different degrees of bone callus formations (Fig. 9; Video 1, 2 and 3, respectively), and larger DS area and levels at mid-proximal than distal rib positions with dark pigments concentrated focally on the affected area (Fig. 9A). This morphological classification (Fig. 9A - C) was positively associated to the general homogeneous appearance of myomere (Fig. 9D - F). Samples showed similar features through micro-CT imaging; fusiform structure of similar radiodensity as near skeletal muscle with some radiopaque islands at continuity breaks (Fig. 9J and K). The sample at mid-proximal rib part showed two rib abnormalities (Fig. 9I); continuity break with no visible callus and diffuse non-mineralized radiolucent callus (Fig. 9L and O); radiopaque callus without visible non-mineralized callus (Fig. 9I and L). Radiolucent structures at the continuity break from inspected samples showed connections with near myomere and transverse fascia (Fig. 9M - O).

Micro-CT of axis deviations in ribs showed alterations of myocommata structure with a tissue of similar radiodensity as skeletal muscle irregularly infiltrated in the myocommata at the axis deviation (Fig. 10D).

Some undetected rib abnormalities from X-ray images were visualized by the 3D model, such as latero-lateral axis deviations, overlapping fractures (Fig. 9F), or bi-tubular rib morphology. Bi-tubular ribs were found to be linked to generalized radiolucent morphology in X-rayed ribs when oriented in the cranio-caudal plane. The generalized radiolucent morphology showed other different forms on the 3D model as thickening with irregular rib lumen, and thinner porotic compact bone

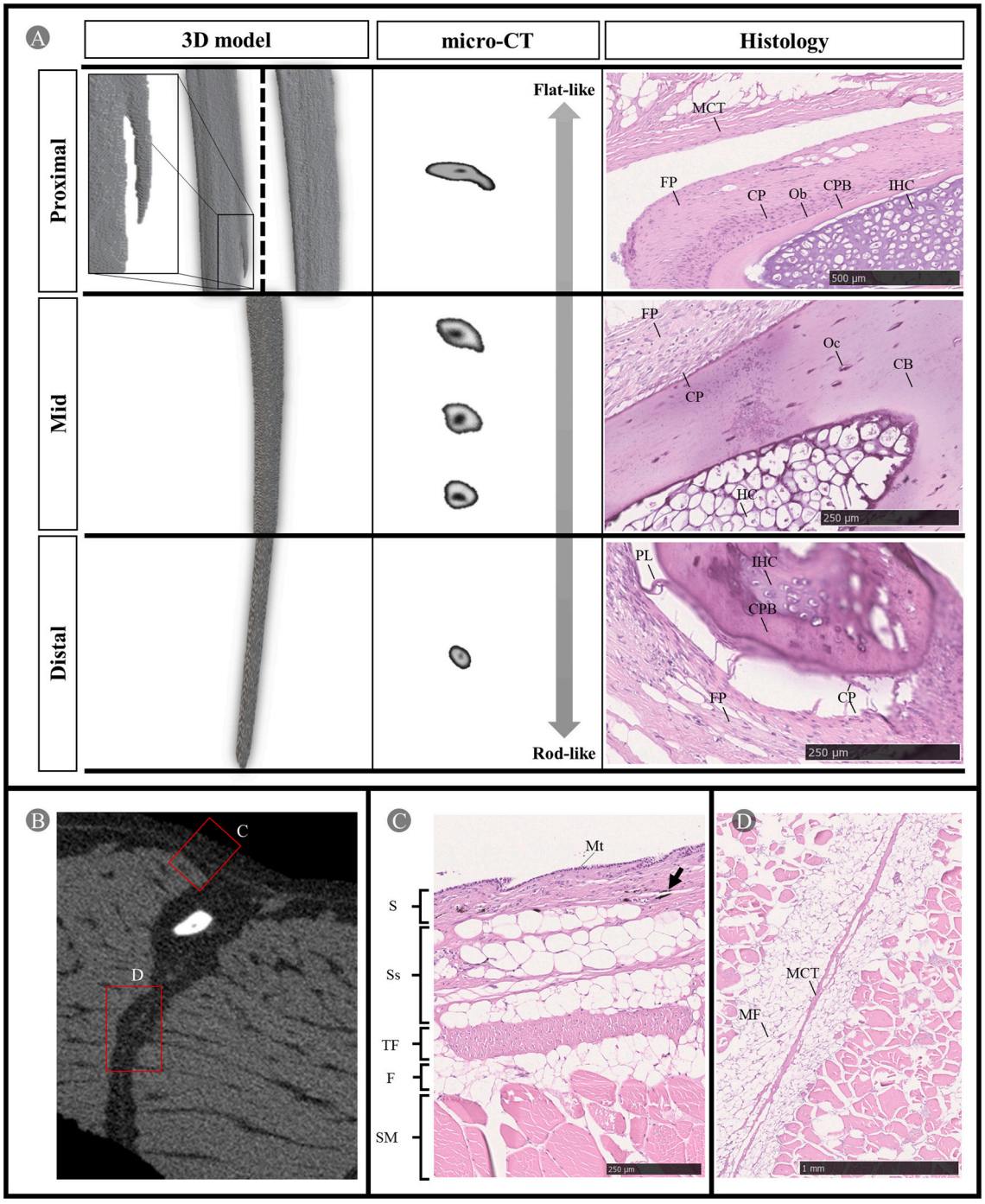

Fig. 8. Anatomical overview of adult Atlantic salmon rib and adjacent structures from targeted rib samples. A) Anatomical description combining 3D model, transversal micro-CT slices and histology at the proximal, mid, and distal rib parts. Box at the proximal area of the 3D model shows a magnified view of the rib process on the external rib side. CB, Compact bone; CP, cellular periosteum; CPB, compact perichondral bone; FP, fibrous periosteum; IHC, immature hyaline cartilage; HC, hypertrophic chondrocytes; Ob, osteoblast; Oc, osteocytes; PL, periosteal ligaments. B) Cross-section micro-CT slice for rib mid part and adjacent structures. Boxes with letters indicate histological illustration of corresponding anatomical regions. C) and D) Anatomical description of adjacent rib structures, both peritoneum and myocommata, respectively, combining transversal micro-CT slice and histology. MCT, myocommata connected tissue; MF, myocommata fat; Mt., mesothelium; S, serosa; SM, skeletal muscle; Ss, Subserosa; TF, transverse fascia; F, fat. Black arrow points to melanomachrophages. Haematoxylin and eosin staining.

cortex of osteolytic and resorptive appearance (Video 4).

3.5. Mineral composition of axial skeleton

Mineral composition of the axial skeleton of slaughter size salmon was similar for salmon farmed in land-based tanks or sea-cages. Wild salmon had significantly lower content than farmed groups for Ca (80,409 ± 3435 vs. 104,165 ± 1692 mg kg^{-1} dw; $p = 0.0001$), P (39,350 ± 1702 vs. 50,979 ± 848 mg kg^{-1} dw; $p = 0.0005$), and Mg (1198 ± 57 vs. 1578 ± 24 mg kg^{-1} dw; $p = 0.0002$). The Ca:P ratio was similar in all groups (2.04 ± 0.01).

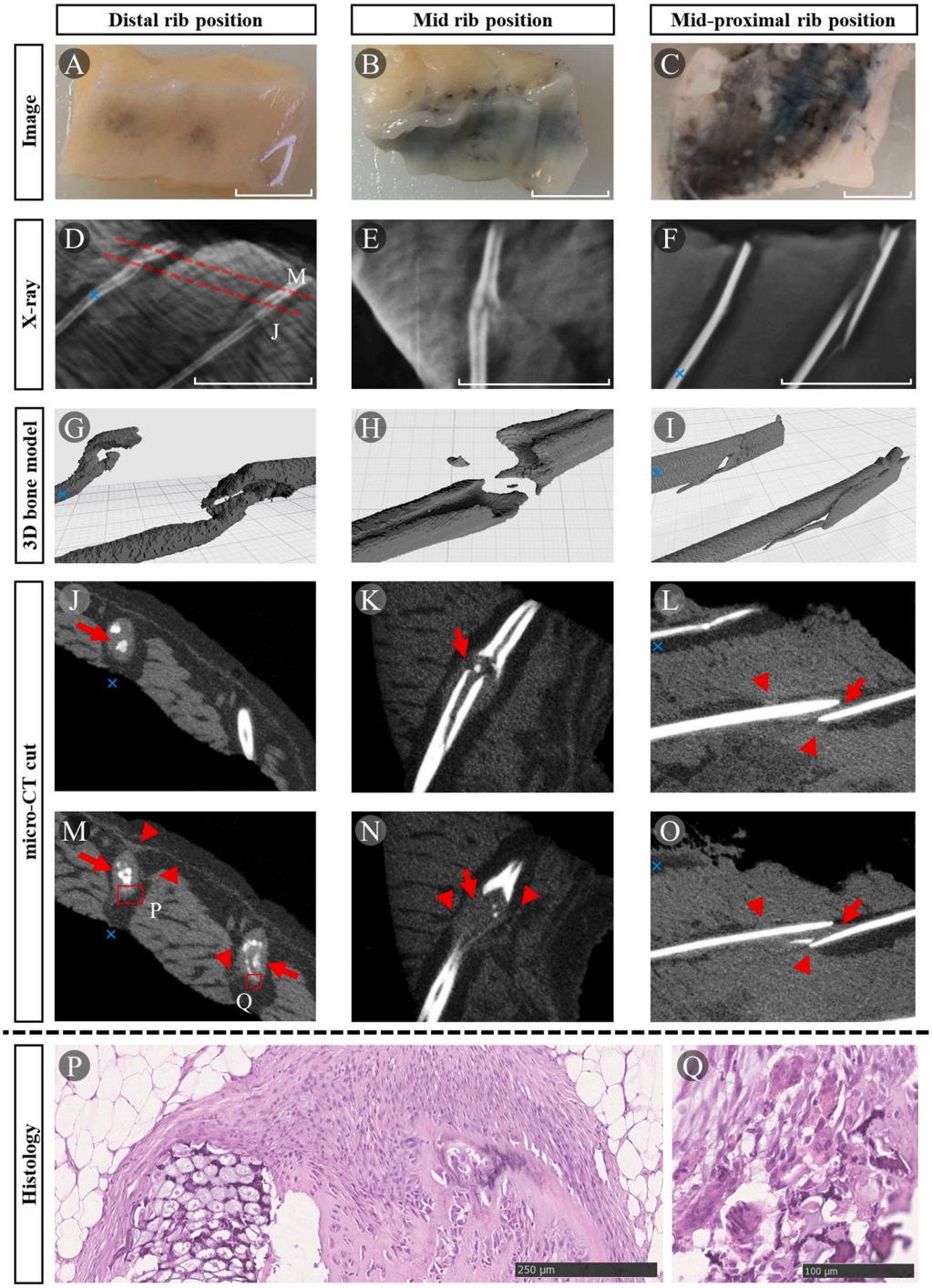

Fig. 9. Characterization of continuity break group abnormalities in targeted focal dark spots (DS) of fillets of farmed Atlantic salmon with different DS levels at different rib parts. Images A) to O) are organized by column. Image, X-ray, 3D model for bone density, and micro-CT cut are provided for each sample. Box with letters on image M) indicates the region of histology P) and Q) (haematoxylin and eosin staining). Parallel discontinuous red lines in X-ray images indicate micro-CT planes if transversal. Blue color marks connect X-ray with micro-CT images. Red arrows point to non-mineralized callus with similar radiodensity as muscle. Red arrowhead indicates the connection between non-mineralized callus and adjacent skeletal muscle or peritoneal transverse facia. Restricted white bars on bottom right corners of A – F show the X-ray and ordinary image scale, set to 1 cm. Major squares in 3D models show the scale, set to 1 * 1 cm. (For interpretation of the references to color in this figure legend, the reader is referred to the web version of this article.)

3.6. Histopathology

The histological morphology of salmon ribs showed a core rich in immature hyaline cartilage in proximal parts, whereas the mid area contained hyaline cartilage in a hypertrophic phase with trabeculae formation. In more distal areas, ribs contained hyaline cartilage (Fig. 8A). Ribs were surrounded by myocommata's connective tissue and located adjacent to the parietal peritoneum, separated by different tissue layers; serosa, subserosa (with visible melanomachrophages), and transverse fascia (Fig. 8B - D). The periosteum presented a series of periosteal ligaments connecting cellular layers with compact rib bone (Fig. 8A).

Histological evaluations of radiolucent fusiform bodies showed signs of external callus formations with hyaline cartilage in several hypertrophic stages non-covered by a compact bone. Fibrous areas with different mineralization degrees were seen near hypertrophic cartilage, whereof trapped active osteoblasts and osteoclasts could be observed (Fig. 9P and Q). The near myomere of mid and mid-proximal DS presented muscle fibrosis and a chronic-active process with melanomachrophage, fat infiltration, and histiocytic-like granuloma formation.

Histology of ribs with axis deviations revealed muscle fibrosis in a chronic-active inflammatory process with melanomachrophage infiltration. Such fibrosis affected the totality of the length of near myocytes. Fat infiltration was observed between muscle fibrosis (Fig. 10E and H).

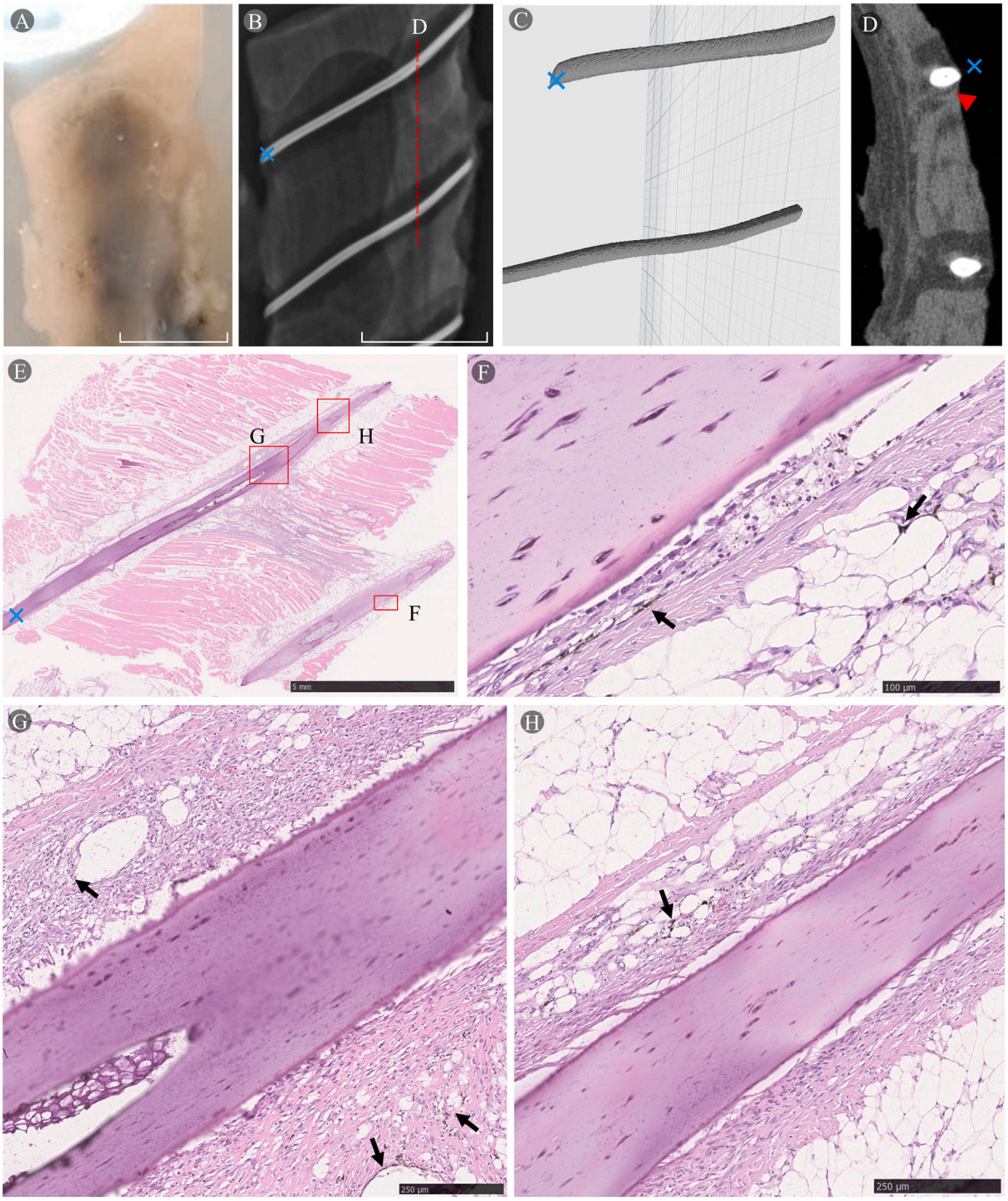

Fig. 10. Characterization of axis deviations in targeted focal dark spots (DS) of fillets of farmed Atlantic salmon shown by A) image, B) X-ray, C) 3D model for bone density, D) micro-CT cut, and E) F) G) H) histology. Blue color mark connects ribs from X-ray to histology images. Boxes with letters on image D) indicate the region of histology of F), G), and H). Discontinuous red line in image B) indicates the micro-CT plane in image D). Red arrowhead indicates the connection between non-mineralized connective tissue around the rib and adjacent structures. Black arrows point to melanomachrophages. The restricted white bar on the bottom right corner of image A) and B) shows the X-ray and ordinary image scale, set to 1 cm. Major squares in the 3D model show the scale, set to 1 * 1 cm. Haematoxylin and eosin staining. (For interpretation of the references to color in this figure legend, the reader is referred to the web version of this article.)

The fibrous periosteum and myocommatas entire architecture from axis deviations were found altered. Metaplastic periosteum with granuloma-like structures and melanomachrophages infiltration between fibrous and cellular layers was observed, giving the periosteum a relatively thicker appearance. Extended vacuolization of cells from the cellular periosteum was also observed, with necrotic melanomachrophage infiltration in some affected areas (Fig. 10F). Periosteal ligaments were found altered (Fig. 10G).

4. Discussion

Fillet-red DS were present in sea-cage farmed salmon throughout the

whole seawater phase as expected (Bjørgen et al., 2019), but the present study is the first to report typical fillet-red DS of the cranio-ventral fillet region of smolts in freshwater. The occurrence of fillet-black DS after five months in seawater coincides with Bjørgen et al. (2019), who proposed that fillet-red DS are acute focal changes that develop into chronic melanized fillet-black DS (Bjørgen et al., 2015). The prevalence of fillet-black DS was 43% on average at harvesting, which is higher than former reports for harvest sized salmon (range 8–33%) (Bjørgen et al., 2019; Dessen et al., 2019; Lutfi et al., 2022; Sissener et al., 2016), though our evaluation method was more sensitive.

The study was initiated with no presumption of the magnitude of morphological rib abnormalities. Hence a consistent deviation from the expected rib morphology of all salmon groups, complicated the understanding of rib abnormality effects on fillet DS. Black DS (either fillet or peritoneum) only occurred in sea-cage farmed salmon, coinciding with twice as high rib abnormalities compared with smolts, salmon farmed in land-based tanks, and wild salmon, however, the association between rib abnormalities and DS is complex. Because all DS were located in the same anatomical area (cranio-ventral), shared healing responses, and rib abnormality types, we assume they share similar ethology with different pathophysiological scenarios. On one hand, muscle strains and hemorrhages (fillet-red DS) of generally round appearance without rib damage, result from either local myositis or traumatic events that exclusively affect soft tissues. Such processes would not be detected by X-ray of the ribs in acute forms, but secondary rib changes may evolve over time when transitioning to fillet-black DS (e.g., generalized radiolucent and shorter or missing rib parts), typically observed at early seawater phase. On the other hand, rib deformations or fractures that evolve into flattened focal lesions, resulting from multiple rib damage in a linear pattern. In this scenario, acute and chronic forms are normally detected by X-ray, unless they are produced in the latero-lateral plane or overlapped, being more typical near slaughter. The presence of ribs with primary and potential secondary changes suggests a combination of both pathophysiologies.

Non-mechanical stress-related forms such as generalized radiolucent could indicate either osteomyelitis (Epsley et al., 2021; Gu et al., 2017), osteoporosis, or osteomalacia. Osteomalacia-derived changes may bring abnormal flexibility (Khurana, 2009), reducing the risk of rib fracture while increasing deformation. However, osteomyelitis and osteoporosis may increase fracture risk. As DS levels depend on the size of the lesion and melanomachrophages density, with a positive trend to muscle fibrosis (by X-ray), this parameter may be a good macroscopic indicator of the focal inflammatory degree, as proposed by Malik et al. (2021). Given the positive association between higher DS levels and the prevalence of generalized radiolucent ribs, focal osteomyelitis is a potential process, as micro-CT analyses suggest.

Similar numbers for most characteristic rib abnormalities in DS between farmed sea-cage salmon rib cages with or without DS, suggest implications of additional major factors than rib abnormalities influencing the development of DS.

Pigmentation of areas of the rib cage under a continuously high degree of motility suggests a natural melanizing response to mechanical stress. Pigmentation related to mechanical stress was likewise present in DS with radiolucent non-mineralized callus, where the chronicity of the histological study indicates abnormal healing responses with delayed mineralization and hypertrophic non-unions (pseudoarthrosis), typical of inadequate stabilization (Khurana, 2009; Kumar et al., 2018; Miclau et al., 2007). Mechanical stress might also cause metaplastic changes resulting in thicker periosteum with altered periosteal unions near axis rib deviation (Sakai et al., 2011). Thus, the degree of mechanical stress in near soft tissue should depend on the type of rib abnormality. On the other hand, distal rib parts, which concentrated most of rib abnormalities, did not coincide with the cranio-ventral fillet region with largest DS, and similar rib abnormalities did not produce the same degree and type of pigmentation at proximal and distal parts. Therefore, there must be other factors contributing to the melanizing response of the healing process in injured tissue.

The flattened cross-sectional rib shape at mid-proximal parts and their deeper location in the muscle wall than in distal rib parts, suggest insertion support for musculature and natural endurance to latero-lateral flexion (Van Leeuwen, 1999). Ribs resist expansion and contraction of fish organs (Jiao et al., 2020), but also oblique and radial expansion of white muscle during explosive starts and turning maneuvers. This concentrates most of the tension at the anterior cones, between mid-proximal rib parts and the horizontal septum (Van Leeuwen, 1999). The association of the higher severity of the spots (larger, more intense, and rounder) at mid-proximal than mid-distal rib anatomical regions evidences such specific mechanical effect on injures, evolving into more severe muscle fibrosis with recurrent injury, chronic-active inflammation (Bjørgen et al., 2019; Larsen et al., 2012; Nikolaou et al., 1987), hypertrophic non-unions (given a rib injury), and pathological interconnections (myofascial adhesions) that increases local stiffness (Bernabei et al., 2017).

While land-based tank smolts were carefully transferred to flow-through seawater tanks and no vaccination was performed, smolts in commercial sea-cages experienced more intensive production-related activities. Such procedures were pumping, grading, vaccination, transportation by well-boat, and mechanical delousing one- and two-months prior harvesting. Additionally, fish in sea-cages experienced different swimming activity, faster growth, and infections (e.g., PRV). There were similar fillet-red DS and rib abnormality types (though in different numbers) in fish from land-based tanks and sea-cages after seawater transfer. Therefore, the absence of melanin during healing in fish from land-based tanks, points to environmental factors as determinants for the final DS phenotype.

Teleost ribs are soft and flexible to sustain constant mechanical loads during swimming (Cohen et al., 2012; Fiedler et al., 2021; Jiao et al., 2020), but in out-of-the-water situations (e.g., grading, vaccination, crowding), fish may experience abnormal forces in either direction or intensity. This migth be seen in the consistent concentration of rib abnormalities in central parts of the rib cage, which reveals a vulnerable area that coincides with the highest occurrence of DS in fillets (rib number 10–14). Nevertheless, no increase in DS and the total number of rib abnormalities after mechanical sea lice treatments was observed. Either delousing did not have an effect on the number of injuries, or there was efficient healing, as the increase of radiopaque callus shows. Although, we must consider a dilution effect of some abnormality types by appositional growth when comparing fish of different sizes.

In view of the abrupt increase in the number of rib abnormalities shortly after transfer to sea-cages, focus on any sources of stress during this period seems justified. The increased number of generalized radiolucent ribs from smolt farm to land-based tanks and sea-cages, suggests a common etiology acting at different magnitudes in both seawater environments. For example, seawater transfer might affect rib bone mineralization in the form of osteomalacia due to different nutritional requirements in response to standard stressful farming procedures (Iversen et al., 2005), not occurring in land-based tanks. Because the mineral composition of the vertebrae was similar for the farmed groups at slaughter and higher than wild salmon, we could exclude general alterations in bone mineralization at slaughter. On the other hand, we should also consider osteomyelitis as a result of inflammatory processes in the muscle wall derived from mechanical stress (e.g., traumatisms) or immune stimulants (e.g., vaccine, infections).

Smolts sampled two weeks after vaccination did not show an increase in the number of rib abnormalities compared to non-vaccinated smolts, even though vaccinated smolts presented fillet-red DS in freshwater. However, the higher numbers of shorter and missing rib parts, and concentration in caudal and distal areas near the vaccination site after transfer to sea-cages, suggest a potential association with vaccination. This fact dissipates the acute effect of a mechanical disturbance of ribs during vaccination and related activities such as pumping and grading. Although, it suggests long-term effects such as alteration of the

path of rib ossification after myotome injury as Akama et al. (2020) reported, and osteomyelitis triggered by the vaccine component or traumatic events between late smolt operations and transfer to sea-cages. The decreasing tendency towards slaughter of shorter or missing and generalized radiolucent ribs highlights the possible effects of production-related factors shortly after transfer to sea-cages, which is considered a particularly critical period in farmed salmon (Bornø, 2021).

Effects of farming operations, such as pumping, grading, and vaccinations on DS in salmon were found negative by Mørkøre (2012). Similarly, Berg et al. (2012) found no cause-effect relationship between vaccine components and DS, although side effects of vaccines on spinal deformities are observed, sometimes co-occurring with focal melanization as part of the inflammatory process (Holm et al., 2020; Trangerud et al., 2020). We found evidence for vaccine-induced rib defects and associated sparse pigmentation, but in line with previous studies, our results can not directly link vaccination component to the presence of DS. However, the presence of histiocytic-like granuloma in fillet-black DS at slaughter was similar to foreign body reactions, as the mineral oil adjuvant used in intraperitoneal salmon vaccines (Carlton et al., 2001; Hwang et al., 2012; Larsen et al., 2012). This might suggest migration of loaded macrophages with vaccine compounds from parietal peritoneum layers (Koppang et al., 2005) to the adjacent skeletal muscle after inflammatory stimuli (e.g., trauma).

Although the salmon farmed in sea-cages showed positive results for PRV, the presence of PRV in sea-cage fish is not considered as the primary cause for DS, since similar Ct-values of PRV were observed in unstained salmon muscle and DS by Mørkøre et al. (2016). Moreover, Bjørgen et al. (2019) did not find PRV in all DS, nor experimental inoculation of salmon muscle caused the development of DS. However, PRV may play a role in modulating the inflammatory response locally (Bjørgen et al., 2019; Krasnov et al., 2016; Malik et al., 2021), as well as other opportunistic pathogens (e.g., *Staphylococcus aureus*) (Tomecka et al., 2019).

The fact that fish farmed in land-based tanks could be exposed to a low concentration of antigenic compounds (no vaccination, UV-treated flow-through water) than in sea-cages (vaccinated, circulating antigens, infections) (Bateman et al., 2021), determines a differential factor for the melanization process in DS. This might be an effect of increased systemic melanin production to enhance immunocompetence to a disease threat, an important component of the innate immune system (Gagnaire et al., 2013; Wilson et al., 2001).

5. Conclusion

Rib abnormalities were common findings in both wild and farmed Atlantic salmon, seemingly a consequence of mechanical stress, and secondary changes due to an inflammatory process. The prevalence doubled after transferring farmed smolts to large commercial sea-cages, coinciding with the presence of fillet-red focal dark spots (DS) and subsequent development of fillet-black DS five months after sea transfer, as opposed to wild salmon and salmon reared in small land-based tanks, that did not develop black DS (either fillet or peritoneum). Rib abnormalities were more prevalent in black DS, and both co-occurred most frequently at the center of the rib cage. The black DS phenotype was associated with a higher presence of rib fractures and rib deformations in the injured area, but DS also occurred without any sign of abnormal ribs or fractures. Other factors such as the anatomical position of the injury contributed to the association. While feed and genetic origin were not primary causes, environmental factors such as damaging incidents in the commercial late smolt phase and sea-cage operations are more likely determinants for the presence of DS.

CRediT authorship contribution statement

Jiménez-Guerrero Raúl: Methodology, Validation, Formal analysis, Investigation, Data curation, Visualization, Writing - original draft, Writing - review & editing. **Baeverfjord Grete:** Conceptualization, Methodology, Validation, Investigation, Resources, Visualization, Supervision, Project administration, Writing - review & editing. **Evensen Øystein:** Methodology, Investigation, Resources, Visualization, Supervision, Writing - review & editing. **Hamre Kristin:** Investigation, Resources, Writing - review & editing. **Larsson Thomas:** Methodology, Investigation, Resources, Data curation. **Dessen Jens-Erik:** Investigation, Resources. **Gannestad Kjellrun-Hoås:** Methodology, Investigation, Resources, Data curation. **Mørkøre Turid:** Conceptualization, Methodology, Validation, Formal analysis, Investigation, Resources, Visualization, Supervision, Project administration, Funding acquisition, Writing - review & editing.

Declaration of Competing Interest

The authors declare the following financial interests/personal relationships which may be considered as potential competing interests:

Turid Mørkøre reports financial support was provided by Norwegian Seafood Research Fund.

Data availability

Data will be made available on request.

Acknowledgments

The Norwegian Seafood Research Fund (FHF) and Norwegian University of Life Sciences (NMBU) supported this study. The study in sea-cages was carried out using Nofima's R&D licenses granted by the Norwegian Directorate of Fisheries for large-scale Industrial Research. The authors acknowledge the skillful assistance and dedicated fish management of the technicians at Lerøy Midt AS, with special thanks to Helge Endresen. The authors remark on the excellent work provided by staff at the Research Station for Sustainable Aquaculture (Nofima) and laboratories. Thanks to Dr. Elisabeth Ytteborg for helping to interpret some results. Thanks to M.Sc. Sumeng Galdat for your assistance processing part of the data. Thanks to Gunhild Haustveit for your help with micro-CT scans during COVID-19 restrictions. Thanks to Professor Øivind Andersen for valuable contributions to the manuscript.

Appendix A. Supplementary data

Supplementary data to this article can be found online at https://doi.org/10.1016/j.aquaculture.2022.738697.

References

Akama, K., Ebata, K., Maeno, A., Taminato, T., Otosaka, S., Gengyo-Ando, K., Kawamura, A., 2020. Role of somite patterning in the formation of Weberian apparatus and pleural rib in zebrafish. J. Anat. 236 (4), 622–629. https://doi.org/10.1111/joa.13135.

Aursand, M., Bleivik, B., Rainuzzo, J.R., Leif, J., Mohr, V., 1994. Lipid distribution and composition of commercially farmed Atlantic salmon (*Salmo salar*). J. Sci. Food Agric. 64 (2), 239–248. https://doi.org/10.1002/jsfa.2740640214.

Baeverfjord, G., Asgard, T., Shearer, K.D., 1998. Development and detection of phosphorus deficiency in Atlantic salmon, *Salmo salar* L., parr and post-smolts. Aquac. Nutr. 4 (1), 1–11. https://doi.org/10.1046/j.1365-2095.1998.00095.x.

Bateman, A.W., Teffer, A.K., Bass, A., Ming, T., Hunt, B.P.V., Krkošek, M., Miller, K.M., 2021. Atlantic salmon farms are a likely source of *Tenacibaculum maritimum* infection in migratory Fraser River sockeye salmon. Can. J. Fish. Aquat. Sci. 00, 1–16. https://doi.org/10.1101/2021.06.15.448581.

Berg, A., Yurtseva, A., Hansen, T., Lajus, D., Fjelldal, P.G., 2012. Vaccinated farmed Atlantic salmon are susceptible to spinal and skull deformities. J. Appl. Ichthyol. 28 (3), 446–452. https://doi.org/10.1111/j.1439-0426.2012.01988.x.

Bernabei, M., van Dieën, J.H., Maas, H., 2017. Altered mechanical interaction between rat plantar flexors due to changes in intermuscular connectivity. Scand. J. Med. Sci. Sports 27 (2), 177–187. https://doi.org/10.1111/sms.12644.

Bjørgen, H., Wessel, Ø., Fjelldal, P.G., Hansen, T., Sveier, H., Sæbø, H.R., Koppang, E.O., 2015. *Piscine orthoreovirus* (PRV) in red and melanised foci in white muscle of

Atlantic salmon (*Salmo salar*). Vet. Res. 46 (1), 89. https://doi.org/10.1186/s13567-015-0244-6.

Bjørgen, H., Haldorsen, R., Oaland, Ø., Kvellestad, A., Kannimuthu, D., Rimstad, E., Koppang, E.O., 2019. Melanized focal changes in skeletal muscle in farmed Atlantic salmon after natural infection with *Piscine orthoreovirus* (PRV). J. Fish Dis. 42 (6), 935–945. https://doi.org/10.1111/jfd.12995.

Bornø, G., 2021. Miscellaneous health problems in farmed salmonids. In: Sommerset, I., Bang Jensen, B., Bornø, B., Haukaas, A., Brun, E. (Eds.), The Health Situation in Norwegian Aquaculture 2020. Norwegian Veterinary Institute.

Carlton, W.W., Boitnott, J.K., Dungworth, D.L., Ernst, H., Hayashi, Y., Mohr, U., Ward, J. M., 2001. Assessment of the morphology and significance of the lymph nodal and hepatic lesions produced in rats by the feeding of certain mineral oils and waxes. Exp. Toxicol. Pathol. 53 (4), 247–255. https://doi.org/10.1078/0940-2993-00198.

Clarke, W.C., Saunders, R.L., McCormick, S.D., 1996. Smolt production. In: Pennel, W., Barton, B.A. (Eds.), Principles of Salmonid Culture. CRC Press, Elsevier, Amsterdam, The Netherlands, pp. 517–567.

Cohen, L., Dean, M., Shipov, A., Atkins, A., Monsonego-Ornan, E., Shahar, R., 2012. Comparison of structural, architectural and mechanical aspects of cellular and acellular bone in two teleost fish. J. Exp. Biol. 215 (11), 1983–1993. https://doi.org/10.1242/jeb.064790.

De Clercq, A., Perrott, M.R., Davie, P.S., Preece, M.A., Wybourne, B., Ruff, N., Witten, P. E., 2017. Vertebral column regionalisation in Chinook salmon, *Oncorhynchus tshawytscha*. J. Anat. 231 (4), 500–514. https://doi.org/10.1111/joa.12655.

Dessen, J.E., Mørkøre, T., Bildøy, J.I., Johnsen, S.N., Poppe, L.T., Hatlen, B., Rørvik, K.A., 2019. Increased dietary protein-to-lipid ratio improves survival during naturally occurring pancreas disease in Atlantic salmon, *Salmo salar* L. J. Fish Dis. 42 (1), 21–34. https://doi.org/10.1111/jfd.12904.

Epsley, S., Tadros, S., Farid, A., Kargilis, D., Mehta, S., Rajapakse, C.S., 2021. The effect of inflammation on bone. Front. Physiol. 11 (1695) https://doi.org/10.3389/fphys.2020.511799.

Färber, F., 2017. Melanin Spots in Atlantic Salmon Fillets – An Investigation of the General Problem, the Frequency and the Economic Implication Based on an Online Survey. Norwegian University of Life Sciences, Ås, Norway.

Fiedler, I.A.K., Elmogazy, O., Courtemanche, G., Cardoso, L., Berteau, J.P., 2021. Bones of teleost fish demonstrate high fracture strain. J. Biomech. 120, 110341 https://doi.org/10.1016/j.jbiomech.2021.110341.

Fjelldal, P.G., van der Meeren, T., Fraser, T.W.K., Sambraus, F., Jawad, L., Hansen, T.J., 2018. Radiological changes during fracture and repair in neural and haemal spines of Atlantic cod (*Gadus morhua*). J. Fish Dis. 41 (12), 1871–1875. https://doi.org/10.1111/jfd.12899.

Fjelldal, P.G., Madaro, A., Hvas, M., Stien, L.H., Oppedal, F., Fraser, T.W.K., 2020. Skeletal deformities in wild and farmed cleaner fish species used in Atlantic salmon *Salmo salar* aquaculture. J. Fish Biol. 98 (4), 1049–1058. https://doi.org/10.1111/jfb.14337.

Gagnaire, B., Cavalie, I., Camilleri, V., Adam-Guillermin, C., 2013. Effects of depleted uranium on oxidative stress, detoxification, and defence parameters of zebrafish *Danio rerio*. Arch. Environ. Contam. Toxicol. 64 (1), 140–150. https://doi.org/10.1007/s00244-012-9814-z.

Gislason, H., Karstensen, H., Christiansen, D., Hjelde, K., Helland, S., Bæverfjord, G., 2010. Rib and vertebral deformities in rainbow trout (*Oncorhynchus mykiss*) explained by a dominant-mutation mechanism. Aquaculture 309 (1), 86–95. https://doi.org/10.1016/j.aquaculture.2010.09.016.

Gu, Q., Yang, H., Shi, Q., 2017. Macrophages and bone inflammation. J. Orthop. Translat. 10, 86–93. https://doi.org/10.1016/j.jot.2017.05.002.

Holm, H., Ytteborg, E., Høst, V., Reed, A.K., Dalum, A.S., Bæverfjord, G., 2020. A pathomorphological description of cross-stitch vertebrae in farmed Atlantic salmon (*Salmo salar* L.). Aquaculture 526, 735382. https://doi.org/10.1016/j.aquaculture.2020.735382.

Horton, J.M., Summers, A.P., 2009. The material properties of acellular bone in a teleost fish. J. Exp. Biol. 212 (9), 1413–1420. https://doi.org/10.1242/jeb.020636.

Hwang, S.H., Kim, H.H., Park, D.J., Jee, Y.S., Lee, K.H., Kim, Y.H., Yang, H.K., 2012. Local tissue reaction after injection of contrast media on gastric wall of mouse: experimental study for application of contrast media to computed tomography lymphography. J. Korean Surg. Soc. 82 (2), 70–78. https://doi.org/10.4174/jkss.2012.82.2.70.

Iversen, M., Finstad, B., McKinley, R.S., Eliassen, R.A., Carlsen, K.T., Evjen, T., 2005. Stress responses in Atlantic salmon (*Salmo salar* L.) smolts during commercial well boat transports, and effects on survival after transfer to sea. Aquaculture 243 (1), 373–382. https://doi.org/10.1016/j.aquaculture.2004.10.019.

Jiao, Y.Y., Okada, M., Hara, E.S., Xie, S.C., Nagaoka, N., Nakano, T., Matsumoto, T., 2020. Micro-architectural investigation of teleost fish rib inducing pliant mechanical property. Materials 13 (22), 5099. https://doi.org/10.3390/ma13225099.

Khurana, J.S., 2009. Bone Pathology, Second ed. Humana Press, Springer, New York, NY, USA.

Koppang, E.O., Haugarvoll, E., Hordvik, I., Aune, L., Poppe, T.T., 2005. Vaccine-associated granulomatous inflammation and melanin accumulation in Atlantic salmon, *Salmo salar* L., white muscle. J. Fish Dis. 28 (1), 13–22. https://doi.org/10.1111/j.1365-2761.2004.00583.x.

Krasnov, A., Moghadam, H., Larsson, T., Afanasyev, S., Mørkøre, T., 2016. Gene expression profiling in melanised sites of Atlantic salmon fillets. Fish Shellfish Immunol. 55, 56–63. https://doi.org/10.1016/j.fsi.2016.05.012.

Kumar, V., Abbas, A.K., Aster, J.C., 2018. Robbins Basic Pathology, Tenth ed (Philadelphia, Pennsylvania, USA).

Larsen, H.A., Austbo, L., Morkore, T., Thorsen, J., Hordvik, I., Fischer, U., Koppang, E.O., 2012. Pigment-producing granulomatous myopathy in Atlantic salmon: a novel inflammatory response. Fish Shellfish Immunol. 33 (2), 277–285. https://doi.org/10.1016/j.fsi.2012.05.012.

Liaset, B., Julshamn, K., Espe, M., 2003. Chemical composition and theoretical nutritional evaluation of the produced fractions from enzymic hydrolysis of salmon frames with Protamex™. Process Biochem. 38 (12), 1747–1759. https://doi.org/10.1016/S0032-9592(02)00251-0.

Lutfi, E., Berge, G.M., Bæverfjord, G., Sigholt, T., Bou, M., Larsson, T., Ruyter, B., 2022. Increasing dietary levels of the n-3 long-chain PUFA, EPA and DHA, improves the growth, welfare, robustness and fillet quality of Atlantic salmon in sea cages. Br. J. Nutr. 1-19 https://doi.org/10.1017/S0007114522000642.

Malik, M.S., Bjørgen, H., Nyman, I.B., Wessel, Ø., Koppang, E.O., Dahle, M.K., Rimstad, E., 2021. PRV-1 infected macrophages in melanized focal changes in white muscle of Atlantic salmon (*Salmo salar*) correlates with a pro-inflammatory environment. Front. Immunol. 12, 664624 https://doi.org/10.3389/fimmu.2021.664624.

Miclau, T., Lu, C., Thompson, Z., Choi, P., Puttlitz, C., Marcucio, R., Helms, J.A., 2007. Effects of delayed stabilization on fracture healing. J. Orthop. Res. 25 (12), 1552–1558. https://doi.org/10.1002/jor.20435.

Mørkøre, T., 2012. Mørke flekker i laksefilet – Kunnskapsstatus og tiltak for å begrense omfanget. Nofima. 17, 1–59.

Mørkøre, T., Larsson, T., Kvellestad, A.S., Koppang, E.O., Åsli, M., Krasnov, A., Rørvik, K. A., 2015. Mørke flekker i laksefilet – Kunnskapsstatus og tiltak for å begrense omfanget. Nofima. 34, 1–79.

Mørkøre, T., Dessen, J.-E., Larsson, T., Jiménez-Guerrero, R., Rørvik, K.-A., 2016. Effekt av fôr på melaninflekker i laks infisert med både PRV og SAV. Nofima. 31, 1–23.

Nikolaou, P.K., Macdonald, B.L., Glisson, R.R., Seaber, A.V., Garrett Jr., W.E., 1987. Biomechanical and histological evaluation of muscle after controlled strain injury. Am. J. Sports Med. 15 (1), 9–14. https://doi.org/10.1177/036354658701500102.

Nordberg, M., 2018. Seasonal Variation in Fillet Quality of Atlantic Salmon (*Salmo salar*). Norwegian University of Life Sciences, Ås, Norway.

Sakai, D., Kii, I., Nakagawa, K., Matsumoto, H.N., Takahashi, M., Yoshida, S., Kudo, A., 2011. Remodeling of actin cytoskeleton in mouse periosteal cells under mechanical loading induces periosteal cell proliferation during bone formation. PLoS One 6 (9), e24847. https://doi.org/10.1371/journal.pone.0024847.

Sissener, N.H., Waagbø, R., Rosenlund, G., Tvenning, L., Susort, S., Lea, T.B., Breck, O., 2016. Reduced n-3 long chain fatty acid levels in feed for Atlantic salmon (*Salmo salar* L.) do not reduce growth, robustness or product quality through an entire full scale commercial production cycle in seawater. Aquaculture 464, 236–245. https://doi.org/10.1016/j.aquaculture.2016.06.034.

Tomecka, M.J., Ethiraj, L.P., Sánchez, L.M., Roehl, H.H., Carney, T.J., 2019. Clinical pathologies of bone fracture modelled in zebrafish. Dis. Model. Mech. 12 (9), dmm037630. https://doi.org/10.1242/dmm.037630.

Trangerud, C., Bjørgen, H., Koppang, E.O., Grøntvedt, R.N., Skogmo, H.K., Ottesen, N., Kvellestad, A., 2020. Vertebral column deformity with curved cross-stitch vertebrae in Norwegian seawater-farmed Atlantic salmon, *Salmo salar* L. J. Fish Dis. 43 (3), 379–389. https://doi.org/10.1111/jfd.13136.

Van Leeuwen, J.L., 1999. A mechanical analysis of myomere shape in fish. J. Exp. Biol. 202 (23), 3405–3414. https://doi.org/10.1242/jeb.202.23.3405.

Wilson, K., Cotter, S.C., Reeson, A.F., Pell, J.K., 2001. Melanism and disease resistance in insects. Ecol. 4 (6), 637–649. https://doi.org/10.1046/j.1461-0248.2001.00279.x.

Zhol, S., Ackman, R.G., Morrison, C., 1995. Storage of lipids in the myosepta of Atlantic salmon (*Salmo salar*). Fish Physiol. Biochem. 14 (2), 171–178. https://doi.org/10.1007/BF00002460.